BOW-SHAPED TOROIDAL FIELD COILS

by

P. Bonanos

PPPL-1790 May 1981

Abstract

Design features of Bow-Shaped Toroidal Field Coils are described and compared with circular and "D" shaped coils. The results indicate that bow coils can produce higher field strengths, store more energy and be made demountable. The design offers the potential for the production of ultrahigh toroidal fields.

Included are representative coil shapes and their engineering properties, a suggested structural design and an analysis of a specific case.

Presented at the 7th International Conference on Magnet Technology, Karlsruhe, F.R.G., March 30 - April 3, 1981.

Bow-Shaped Toroidal Field Coils

Peter Bonanos

Plasma Physics Laboratory, Princeton University
Princeton, New Jersey 08544

Introduction

The maximum field which can be produced in a toroidal coil is usually determined by a limiting tensile stress reached at the inner major radius R_1. In Ref. 1 a structural arrangement, termed a "bow coil," was described which permits a reduction in the tension at the inner radius. A fuller and more general description is presented here and compared with other forms of toroids. Performance limits are estimated and useful engineering parameters are tabulated. A simple structural analysis is also included to demonstrate the mechanical behavior of practical coils.

General Mechanics

The total vertical force on each half-coil of a toroidal array is given by

$$P = \frac{1}{2} I B_0 R_0 \ln R_2/R_1 \qquad (1)$$

where I is the coil current and B_0R_0 the field-radius product at some internal point. It is independent of the coil shape.[2]

#81E0042

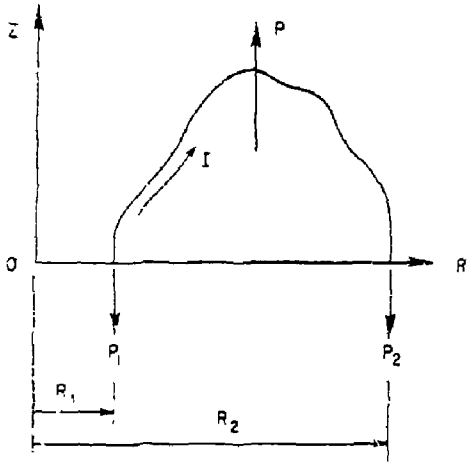

Fig. 1 Vertical Coil Forces

The sum of the reaction forces P_1 and P_2 must of course, equal P. Their respective values however are functions of the coil aspect ratio A equal to $(R_2 + R_1)/(R_2 - R_1)$ and the structural support arrangement.[3] Since the cross-sectional area available to support tension is less at R_1 than at R_2, methods of reducing $f_p \equiv P_1/P$ are sought. For circular coils having useful aspect ratios this fraction has a range $0.6 \lesssim f_p \lesssim 0.7$. For constant tension coils[1] $f_p = 0.6$.

The structural arrangement shown in Fig. 2 can further reduce f_p.

#81E0040

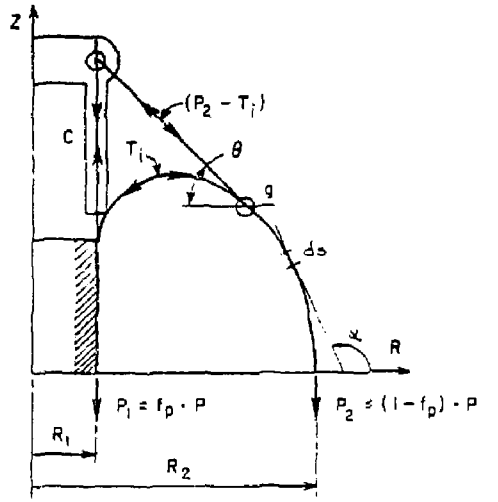

Fig. 2 Bow Coil Arrangement

A tension link is attached to each coil at q with inclination angle θ and tangent to the coil. The links are attached to a central cylinder which transmits a compressive force C directed towards the midplane. The compression C reduces the coil tension at R_1 and, through the links, increases the tension at R_2. If viewed in a literally global sense, the equatorial pressure in the toroid is used to produce compression from pole to pole.

Bow Coil Shapes

A coil shape can be generated using connected, constant tension, arc segments[1] if

$$\rho = ds/d\alpha = T/\sigma \qquad (2)$$

where ρ is the radius of curvature, T the tension and σ the load per unit length of arc ds. Using the thin-shell approximation for the toroidal field, $B = B_0R_0/R$, the unit load is $\sigma = I B_0R_0/2\pi R$. For the outer arc of the coil at R_2 where the tension is $T_2 = (1 - f_p)P$ the curve, using Eqs. (1) and (2), is given by

$$ds/d\alpha = (1 - f_p) R \ln (R_2/R_1) . \qquad (3)$$

The tension within the inner, curved portion of the coil (between g and R_1) is T_1. The tension in the link is then $(P_2 - T_1)$. The force in the straight portion of the coil at R_1 is then

$$P_1 = f_p P = T_1 + (P_2 - T_1)\sin\theta \,. \qquad (4)$$

Combining (1), (2), and (4) the inner curve of the coil is given by

$$ds/d\alpha = \frac{f_p + (1 - f_p)\sin\theta}{1 + \sin\theta} R \ln(R_2/R_1) \,, \qquad (5)$$

and the link tension is

$$P_2 - T_1 = P[1 + 2f_p)/(1 + \sin\theta] \,. \qquad (6)$$

Since coil stresses are constant for a given field strength and aspect ratio it is convenient to normalize the geometry using a unit average radius $R_0 = (R_1 + R_2)/2 = 1$ and the *inverse aspect ratio* (i.e., toroidicity) $\epsilon = (R_2 - R_1)/(R_1 + R_2) = 1/A$. The shapes for constant f_p and varying θ are shown in Fig. 3.

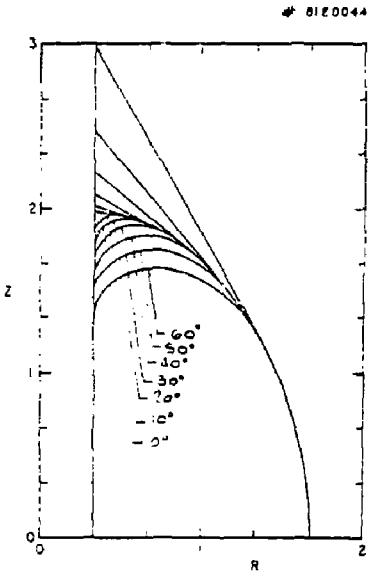

Fig. 3. Coil shapes for $f_p = 0$, $\epsilon = 2/3$ and $0 \le \theta \le 60°$ in steps of 10°

The shapes for constant θ and varying f_p are shown in Fig. 4.

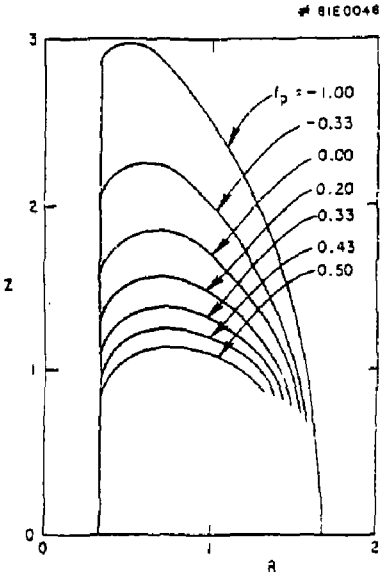

Fig. 4 Coil Shapes for $\theta = 45°$, $\epsilon = 2/3$ and $-1 \le f_p \le 0.5$.

Coil Characteristics and Performance

To evaluate coil performance some additional geometry (Fig. 5) is now defined.

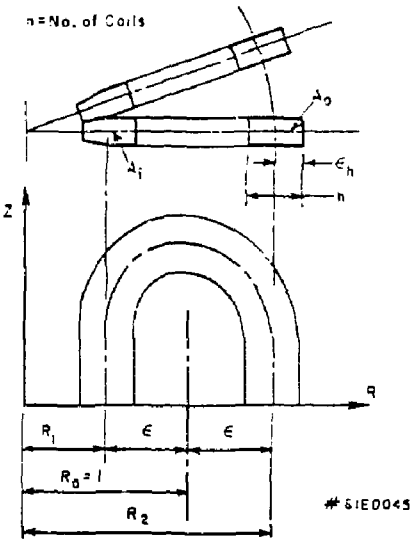

Fig. 5 Coil Geometry

The inner cross section A_1 is partitioned such that 1/3 A_1 is devoted to insulation and coolant. The remainder is available to support forces and the sum for all coils is equal to $3\pi\epsilon_h(1-\epsilon)/3$ where ϵ_h is the radial half-thickness. At the outer radius R_2 an opacity defined as $nA_2/2\pi R_2 h$ is taken to be 1/3 (the figure is drawn to scale). The area for insulation and coolant is assumed constant throughout the coil length. The total net area at R_2 is then $n(A_2 - A_2/3) = 3\pi\epsilon_h/3$.

Using $BR = \mu_0 n I/2\pi$ (MKS) and converting (1) to the present notation, the vertical coil force sum is

$$\Sigma F = \frac{\pi B_0^2}{\mu_0} \ln\left(\frac{1+\epsilon}{1-\epsilon}\right) . \qquad (7)$$

A tensile force corresponding to 100 MPa (14.5 ksi) on the net area is now allowed. If the field strength is limited by the inner cross section (at R_1) then, from (7), the maximum value at R_0 is

$$B_{0_1} = \left[\frac{320\ \pi}{3}\ \frac{\epsilon_h(1-\epsilon)}{f_p \ln\left((1+\epsilon)/(1-\epsilon)\right)}\right]^{1/2} . \qquad (8)$$

If limited by the net cross section at R_2 then

$$B_{0_2} = \left[\frac{320\ \pi}{3}\ \frac{\epsilon\ \epsilon_h}{1 - f_p \ln\left((1+\epsilon)/(1-\epsilon)\right)}\right]^{1/2} . \qquad (9)$$

The total field energy W and inductance L are related by

$$W = \frac{1}{2\mu_0}\int_V B^2\,dV = \frac{1}{2} L I^2 . \qquad (10)$$

If a thin shell is again assumed then, for $B_0 = \text{Tm}$,

$$W = \frac{2\pi}{\mu_0} B_0^2 \int_{-z}^{+z} \frac{z\,dR}{R} \text{ joules},$$

and the single-turn inductance (MKS) is given by

$$L = \frac{2\pi}{I^2} \int_{1-\epsilon}^{1+\epsilon} \frac{z\,dr}{R} \text{ henries}.$$

Four coil shapes are now compared: (1) Circular Coils, (2) Constant Tension Coils, (3) Constant Stress Bow Coils, and (4) Demountable Bow Coils.

For the circular coils a support scheme is assumed such that the in-plane moments are negligibly small and the point of zero moment is at R_2 (or nearby) so that f_p may be estimated. A low moment is admittedly difficult to achieve but toroids such as TFTR attempt this objective.[5]

For the constant stress bow coil the tensile stresses at R_1 and R_2 are set equal (but the effective stresses $\sigma = \sigma_{max}$ are not). The necessary fraction f_p is then a function of the net cross sections and the toroidicity. For the assumed packing fraction and transparency $f_p = 1 - \epsilon$.

For the demountable toroid f_p is set equal to $1 - 1.1\epsilon$. The coil joints are assumed to be in the straight portion of the coil at R_1 and 10% of the total vertical force is applied compressively.

The results are shown in Fig. 6 (next page) for toroidicities $0.5 < \epsilon < 0.8$, and radial half-thicknesses $\epsilon_h = 0.1$, 0.2 and 0.3. For the bow coil examples θ is always 45°. Note that the "D" coil and constant stress bow coil are identical for $\epsilon = 0.5$. Representative values are also listed in Table I.

Structural Analysis

Two practical problems are now addressed (1) The effect of deformations (in both the coil and structural supports) on the internal force distribution, and (2) A realizable structure equivalent to the schematic arrangement shown in Fig. 2.

The cylinder and pinned link configuration is difficult to construct due to the congestion where the links converge. The inverted arrangement shown in Fig. 7 is simpler. The coil structure is extended axially in the shape of a triangular blade (B) and a massive ring (A) restrains the radial motion. The blade then pushes towards the midplane at R_1.

A coil shape was generated for $\epsilon = 0.7$ $\epsilon_h = 0.2$ and $f_p = -.2$. A structural model is shown in Fig. 8. The analysis, using a structural code,[6] indicates that distortions reduce the compressive force at R_1 to $f_p = -0.17$. All forces are within ~ 5% of the predicted values.

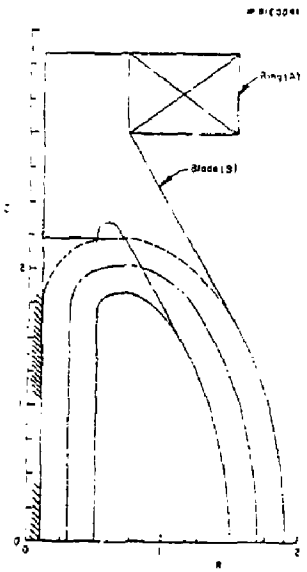

Fig. 7 Arrangement of Structural Support

	Circular Coils				Dee Coils					Constant Stress Bow Coils					Demountable Bow Coils				
ϵ =	0.5	0.6	0.7	0.8	ϵ =	0.5	0.6	0.7	0.8	ϵ =	0.5	0.6	0.7	0.8	ϵ =	0.5	0.6	0.7	0.8
Mean Length	3.14	3.77	4.40	5.03		4.08	5.21	6.53	8.15		4.08	5.65	7.65	10.3		6.06	7.77	9.76	12.2
Volume	4.93	7.11	9.67	12.6		7.36	11.4	16.7	23.9		7.36	12.8	20.5	31.6		12.3	18.7	27.0	38.0
Z Max.	0.50	0.60	0.70	0.80		0.74	0.97	1.25	1.61		0.74	1.09	1.56	2.19		1.28	1.67	2.13	2.72
L-Single Turn	0.17	0.25	0.36	0.50		0.28	0.47	0.77	1.27		0.28	0.53	0.96	1.73		0.49	0.81	1.31	2.14
f_p	0.59	0.61	0.64	0.67		0.50	0.50	0.50	0.50		0.50	0.40	0.30	0.20		-0.1	-0.1	-0.1	-0.1

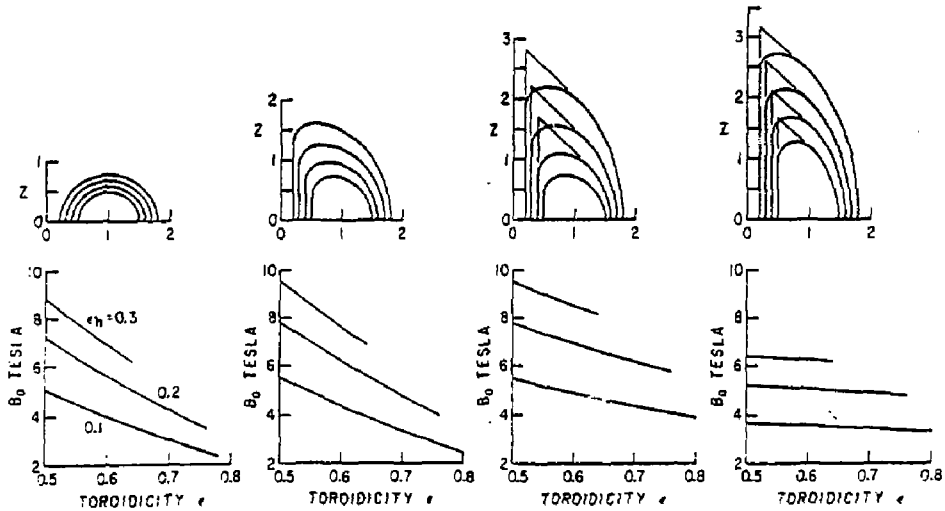

Fig. 6 Comparison of Coil Shapes. The single turn inductance assumes R_o = 1 meter and is in microhenries.

		Circular		Dee		Constant Stress		Demountable	
ϵ	ϵ_h	B_o T	W Mj	B_o T	W Mj	B_o T	W Mj	B_o T	W Mj
0.5	.1	5.1	54	5.3	106	5.5	106	3.7	84
	.2	7.2	109	7.8	212	7.8	212	5.3	169
	.3	8.8	163	9.6	318	9.6	318	6.5	253
0.6	.1	4.0	50	4.4	113	4.9	160	3.6	133
	.2	5.6	99	6.2	226	7.0	320	5.1	266
	.3	6.9	149	7.6	339	8.5	480	6.3	399
0.7	.1	3.0	41	3.4	111	4.4	232	3.5	200
	.2	4.3	82	4.8	222	6.2	463	5.0	401
0.8	.1	2.8	39	3.2	109	4.3	249	3.5	217
	.2	4.0	77	4.6	219	6.1	497	4.9	434

Table I. Selected values of maximum field at R_o and Stored Energy.

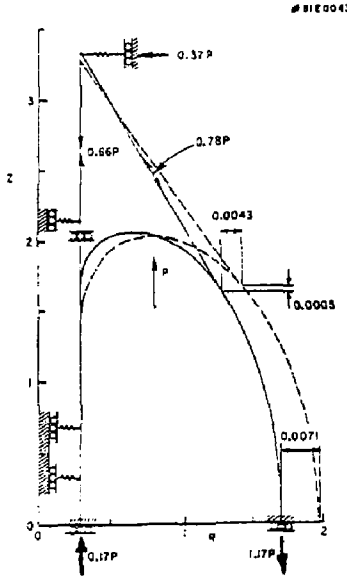

Fig. 3 Structural Model. The distortions are fractions of R_o and are shown exaggerated.

Conclusions

The "D" and Bow Coil can produce higher fields and stor more energy than can circular coils. Demountable, high field coils can also be constructed. Coil distortions affect the load distributions and, in simple models, require small adjustments. In practice, however, careful design of details is important since small deflections in large structures affect the result. The retaining ring and blade for example, must include an adjustment scheme (i.e., wedges) to remove free play or apply a preload.

For the special case $f_p = 0$ the straight portion of the coil must support the centripetal force alone; this suggests a "thin" particle detection magnet for high energy physics research with a completely open toroidal field volume.

With its' higher field capability the constant stress bow coil is the most effective energy storage device. Note, however, that this result is based on the restrictive condition that the coil system be transparent at R_2. If λ_o is increased and $f_p \approx 0$, yet higher fields can be produced. The upper limit has not been examined. The particular case $t \approx R_o$, $f_p \approx 0$ may provide interesting results.

Acknowledgments

I thank Fred Tenney for his advice, encouragement and technical review and Jack Joyce for his support.

References

[1]P. Bonanos, "Bow-Shaped Toroidal Magnet Coils," Plasma Physics Laboratory Report PPPL-1708, Sept. 1980. To be published in Review of Scientific Instruments.

[2]D. W. Weissenberger, J. R. Christensen and J. Bialek, "The Pure Tension Shape of a Thick Torus," Plasma Physi s Laboratory Report, PPPL-1353, July 1977.

[3]J. File, R. G. Mills, and G. V. Sheffied, "Large Superconducting Magnet Designs for Fusion Reactors," Plasma Physics Laboratory Report MATT-848, June 1971.

[4]S. L. Gralnick and F. H. Tenney, J. Appl. Phys., 47, (1976) p. 2710.

[5]L. Blumenau, J. Citrolo, J. Bialek, and G. Cargulia, "TFTR Coil Support Restraint Structure," Proceedings of the 8th Symposium on Engineering Problems of Fusion Research, Nov. 1979, Vol. I p. 113.

[6]ICES Strudl-II the Structural Design Language Vol. 1, Nov. 1968 MIT, Department of Civil Engineering, Cambridge, Mass.